HHS Public Access

Author manuscript

Magn Reson Med. Author manuscript; available in PMC 2017 April 01.

Published in final edited form as:

Magn Reson Med. 2016 April ; 75(4): 1565–1573. doi:10.1002/mrm.25751.

B_1 and T_1 mapping of the breast with a reference tissue method

Federico D Pineda[*], **Milica Medved**, **Xiaobing Fan**, and **Gregory S Karczmar**[*]

Department of Radiology, University of Chicago, Chicago, IL

Abstract

Purpose—To develop a method for mapping the B1 field using a reference signal from a tissue with known T1.

Methods—Flip angle correction factors were calculated in a region with a known 'gold standard' T1; by comparing T1 values from a variable flip angle (VFA) sequence to the 'gold standard' and correcting the value of the Ernst angle. The resulting partial B1 map was interpolated for all other regions. In the breast, fat is an ideal reference tissue because its T1 is spatially homogeneous and inter-patient variability is low. This method was tested with scans of phantoms and patients (n=4) on a 3T magnet. The performance of the method was evaluated by comparing the results of VFA T1 mapping with and without B1 correction to inversion recovery (IR) T1 maps.

Results—Phantom data determined that a linear inverse distance weighted interpolation accurately recovered the full B1 map. Use of interpolated maps to correct the VFA data in-vivo, reduced the average difference in the T1 of parenchyma between VFA and IR results from 58% to 8%.

Conclusions—This proof-of-principle study showed that it is possible to recover a full and accurate map of the B1 field in the breast by using a reference tissue (fat) with an accurately measured T1.

Keywords

B_1 map; reference tissue method; quantitative breast imaging; T_1 mapping

Introduction

Dynamic contrast enhanced MRI (DCE-MRI) is a highly sensitive method for the detection of breast cancer (1–3). During a DCE-MRI exam a series of T_1-weighted images are acquired before and after the intravenous injection of paramagnetic contrast media. The contrast agent preferentially accumulates in lesions due to their increased blood flow and fenestrated (leaky) vasculature, increasing their signal intensity in a T_1-weighted image. Routine analysis of DCE-MRI of the breast involves the tracking of signal increase and decrease in tissues indicative of the uptake and washout of contrast media (4).

[*]Corresponding Authors: Department of Radiology, MC2026, The University of Chicago, 5841 South Maryland Avenue, Chicago, IL 60637. Voice: (773) 834-7769, FAX: (773) 702-0371, gskarczm@uchicago.edu (GK) or fdp@uchicago.edu (FP).

B_1 inhomogeneity is especially notable in breast MRI, due to the large fields-of-view (FOV) required for bilateral breast imaging, and the off-center positioning of patients in the coil. Kuhl et al. reported significant differences in the B_1 field across the FOV, with differences of nearly a factor of two between the left and right breasts (5). These differences can lead to variations in image intensity across the FOV (e.g. shading), as well as spatial variations in the signal enhancement in lesions after the administration of a contrast agent. Azlan et al. mapped the B_1 field in several healthy volunteers at 3 Tesla (T) and simulated differences in enhancement in a phantom study (6). They found significant differences between the right and left breasts, and reductions of more than 50% of the nominal B_1 in some cases. They also showed that a reduction in B_1 leads to a reduction of the enhancement ratio (ER), possibly reducing the conspicuity of a breast lesion.

Dual source, parallel radiofrequency (RF) excitation has been proposed as a method of reducing variations in the B_1 field (7). Rahbar et al. compared B_1 maps acquired in the breast using both single and dual source RF excitation (8). They found that while the use of dual source parallel excitation reduced differences in the whole breast mean B_1 value between the right and left breasts compared to single source excitation, significant differences remained at some locations even when parallel excitation was used.

B_1 field inhomogeneity has a significant effect on the estimation of quantitative parameters in DCE-MRI (9). Estimations of native T_1's of tissues, using a variable flip angle approach, rely on the accurate knowledge of the flip angles used. Knowledge of the native T_1 as well as the actual flip angle is necessary for an accurate estimate of post contrast T_1 based on signal enhancement in DCE-MRI. Measurements of contrast agent concentration are obtained from the native and post-contrast T_1's, and thus are affected by the errors in the estimated flip angle in the region-of-interest (ROI). In fact, when the repetition time is short, and a low flip angle is used; a small error in the flip angle can lead to a large bias in concentration. In DCE-MRI of the breast it is common to use protocols with these conditions (at our institution for example standard protocols include a TR of 5 ms and flip angle of 10°). For this reason accurate knowledge of the actual flip angle is essential for accurate measurements of contrast media concentration, a necessary step in the measurement of pharmacokinetic parameters of lesions (e.g. K_{trans}, v_e, and k_{ep}) (10,11).

The issues outlined above demonstrate the need for methods for accurate mapping of the B_1 field *in vivo* for research applications and clinical evaluation of DCE-MRI images. The actual flip angle imaging (AFI) method can be used to measure B_1 maps *in vivo* (12). In this approach the ratio of the signal at two different repetition times (TRs) is used to derive the actual flip angle in each voxel. When implementing this sequence one must ensure that the transverse magnetization is adequately spoiled, and that the steady state has been achieved, otherwise the accuracy of the AFI technique is affected (13). Additionally, large flip angles are required when implementing this sequence, this leads to a reduced signal-to-noise ratio, potential artifacts from stimulated echoes, and a distortion of slice profiles. Furthermore, this sequence may not be available depending on the particular vendor/scanner used and its implementation may require pulse programming knowledge. Other methods for *in vivo* B_1 mapping include the saturated double-angle method (SDAM) (14), dual refocusing echo acquisition mode (DREAM) (15), and mapping by Bloch-Siegert shift (16). In a study by

Nehrke et al. RF shimming with DREAM, AFI and SDAM was compared (17). The authors found that DREAM outperformed the other methods while significantly reducing acquisition time. Bloch-Siegert shift B_1 mapping offers the advantage of insensitivity to factors such as TR, T_1, and flip angle (DREAM has a weak dependence on T_1 and T_2). In fact, there is potential to combine DREAM and Bloch-Siegert approaches to produce a new and more accurate method. One drawback of the DREAM and Bloch-Siegert B_1 mapping methods is that they require specialized sequences that are implemented through research software patches (which are not widely available).

Here we present an approach for accurately mapping B_1 and T_1 values in the breast, with a variable flip angle (VFA) sequence and use of adipose tissue in the breast as a reference tissue. As demonstrated by Sung et al. fat is an ideal T_1 reference tissue for breast imaging (18). Rakow-Penner et al. used a fast spin-echo inversion recovery technique to accurately measure the T_1 of fat in the breast and found a mean value of 367 ms ± 8 ms at 3T (19). Merchant et al. also reported a low standard deviation in the T_1 of fat in the breast at 1.5T, with an average value of 265 ms ± 2 ms (20). Graham et al. measured the fat T_1 in *ex-vivo* samples and found an average value of 230 ms ± 10 ms (21). The relatively low standard deviation in these studies suggests a low variability in the T_1 value of fat, both inter-patient and across the breast (values at 3T were measured in several ROIs in each patient). By measuring the T_1 of the fat in the breast of a patient, or, assuming low inter-patient variability, using a population based value for the T_1 of fat, it is possible to find the actual flip angle in each fat voxel. The method presented here allows for B_1 mapping of the breast based on standard T_1 mapping sequences.

Methods

Theory

T_1 was estimated by fitting variable flip angle (VFA) data from each voxel to the spoiled gradient echo signal model (22):

$$S = M \quad sin \quad \alpha \frac{1 - e^{-TR/T_1}}{1 - cos \quad \alpha e^{-TR/T_1}} \quad (1)$$

The optimal fits based on the nominal flip angles (those prescribed at the scanner console) provide an estimate of T_1 in each voxel. In the presence of an inhomogeneous B_1 field differences between the estimated and actual T_1 can be attributed, in part, to differences between the nominal and actual flip angles. In each voxel in the reference tissue (where the actual T_1 is known) a proportionality factor ‘A’ can be calculated to correct for differences in the flip angles:

$$\alpha' = A\alpha \quad (2)$$

Where α’ is the actual flip angle, α is the nominal flip angle. A is assumed to be constant at a particular location for the range of relatively small flip angles used here, and proportional

to B_1 (23). 'A' can be defined as the ratio of the Ernst angle for the true T_1 to the Ernst angle for the measured T_1 from the fit to equation (1) with the nominal flip angles:

$$A=\frac{\theta_{Et}}{\theta_{Em}}=\frac{cos^{-1}\left(e^{-TR/T_{1t}}\right)}{cos^{-1}\left(e^{-TR/T_{1m}}\right)} \quad (3)$$

Where θ_E is the Ernst angle and the subscripts t and m denote the true and measured T_1 values, respectively.

The map of 'A' or B_1 must then be estimated for all image voxels to obtain a correction to the nominal flip angle. To do this we developed the interpolation procedure outlined below.

B_1 map interpolation

After a VFA volume is acquired and fit to the spoiled gradient echo signal model, as detailed above, the following steps were taken to obtain a B_1 map for the whole breast.

1. Segment the fat in the image by thresholding the uncorrected T_1 map (since the T_1's of glandular tissue are significantly longer than those of fat). A signal intensity threshold can also be used on one of the VFA images where there is good visual differentiation between fat and glandular tissue. Segmentation was supervised to account for signal intensity variation due to the inhomogeneous B_1 fields of the excitation and receiver coil.
2. A T_1 for fat can be measured very accurately at a few points using spectroscopic 'recovery from inversion' methods. Since the fat T_1 is very homogeneous, the T_1 found in a few (or one) fat regions can be assumed to apply to all fat voxels. In principle a 'population' value for the fat T_1 can be used as a reference.
3. Solve Equation (3) for each fat voxel, using the uncorrected T_1 values, and the gold standard value for the fat T_1.
4. Identify the regions with missing B_1 values (i.e. non-fatty regions of the breast) using a region labeling algorithm.
5. For each voxel in the regions of the B_1 map that need to be filled, identify the nearest 'N' neighbors with B_1 values in each 8-connected direction, along with the Euclidean distance between the voxel and each of the neighbors.
6. Interpolate to estimate the missing B_1 value $B_1(x,y)$ from its nearest neighbors using inverse distance weighting.

$$\boldsymbol{B}_1(x,y)=\frac{\Sigma_{i=1}^{N} w_i(x,y)\, B_1(x_i,y_i)}{\Sigma_{i=1}^{N} w_i(x,y)} \quad (4)$$

Where N is the number of neighbors being used, x_i are the voxel locations with known B_1 values $B_1(x_i,y_i)$ and w_i are the distance weights being used and given by:

$$w_i = \frac{1}{{d_i}^P} \quad (5)$$

d_i is the Euclidean distance between voxels (x,y) and (x_i,y_i) and P is the power of the distance weighting.

7. Repeat steps 5 and 6 for all voxels and regions.
8. Apply an averaging filter to the resulting map to smooth the B_1 map.

The optimal values of N (number of neighbors used in the interpolation) and P (the power of the distance weighting) were determined in phantom scans described below. Segmentation of the fat in the image must be performed with care so as not to include partial volume voxels at the boundaries between fat and glandular tissue as this could lead to artificially large gradients in the B_1 map at these locations.

The result of this algorithm is a complete B_1 map of the whole breast, where the values of B_1 in glandular tissue were interpolated from the values in the surrounding fat voxels.

Phantom Scans

All scans were performed on a Philips Achieva 3.0T TX scanner (Philips Healthcare, Best, The Netherlands) using a 16-channel bilateral breast coil (MammoTrak), and dual source parallel RF excitation (MultiTransmit).

To investigate the feasibility of the approach outlined above, and to determine adequate values for ‘N’ and ‘p’ in equations (4) and (5), respectively, we scanned a breast flood phantom. The flood phantom consisted of a mixture of water and $CuSO_4$. Previous experiments on this phantom showed a gradient in the B_1 field ranging from roughly 70% to 130% of the prescribed flip angle, thus the phantom provides a reasonable test for this method. The T_1 of the phantom was measured using a single voxel PRESS preceded by an inversion pulse and the following acquisition parameters: 5 mm isotropic voxel; TR/TE = 5100/36 ms; inversion delays of 50 ms, 200 ms, 500 ms, 1000 ms and 3000 ms; number of samples averaged (NSA) = 4. This sequence was repeated at four different locations in the flood phantom. The VFA sequence consisted of a 3D spoiled gradient echo (fast field echo), TR/TE = 10/2.4 ms; 2 mm isotropic acquisition voxels; NSA = 2; flip angles = 5°, 10°, 15°, 20°. An actual flip angle (AFI) B_1 map was also acquired using a dual TR acquisition with TR_1 = 10 ms; TR_2 = 50 ms; voxel size 5 mm × 5mm; 10 mm slice thickness; and a flip angle of 60°.

Data analysis was performed in Matlab (MathWorks, Natick, MA) with in-house built software. The VFA data were fit to the signal model shown in Equation (1), and a T_1 map of the flood phantom was generated. This map, along with the true T_1 from the spectroscopic sequence were then used to create a B_1 map by solving Equation (3) for each voxel. The flip angle of the inversion pulse was assumed to be fixed at 180° when fitting the IR data. Because the phantom being scanned consisted of a uniform solution, the resulting map included the whole phantom.

To evaluate the accuracy of an interpolated map, regions were drawn and zeroed out from the B_1 map of the phantom. The B1 map of the remainder of the phantom was then interpolated using the code described above, with varying values of the power of the inverse distance weights (P) and the number of neighbors used for the interpolation (N) of each voxel. The resulting interpolated maps were then compared to the original full B_1 map to determine the best combination of P and N. Values of N tested ranged from 1 to 8, while the P's tested were 1, 2 and 3. This was repeated for regions of different sizes and shapes.

We built a second phantom to mimic the magnetic properties of tissues in the breast, as described by Liney et al. (24). The phantom consisted of lard and gelatin, to mimic breast fat and parenchymal tissue, respectively. In the middle of the phantom, we placed a small vial containing a mixture of water and gadobutrol (Gadavist, Bayer, Whippany, NJ). The phantom was placed into the right breast cup of the bilateral breast coil. Cross-sections of this phantom can be seen in Figure 1. A VFA sequence was acquired, with the same acquisition parameters as described for the flood phantom. An inversion recovery fast spin-echo (IR-FSE) sequence was also acquired with the following parameters: TR/TE = 9000/36 ms; 2 mm isotropic voxels; inversion times: 50, 150, 300, 600, 1000, 3000 and 4000 ms. In this phantom, the lard was used as the reference "tissue". Its true T_1 value was calculated from the inversion recovery sequence. The B_1 map was created from the VFA data as described above, using the lard as the reference signal and interpolated in the other areas, and used to correct the VFA T_1 map. The accuracy of the corrected T_1 map (using the interpolated B_1 map) was evaluated using the inversion recovery T_1's as the gold standard.

In vivo Scans

The methods presented here were evaluated in four patient scans (ages: 23, 28, 51, and 52), with the same scanner and coil used in the phantom scans. Informed consent was obtained under an IRB-approved, HIPAA-compliant protocol. A 3D VFA volume was acquired with the following acquisition parameters: 1 mm isotropic voxels; TR/TE = 10/2.4 ms; flip angles = 5°, 10°, 15°, and 20°; acquisition time of roughly 1.5 min for each flip angle. An IR-FSE sequence was acquired with: TR/TE = 5000/32 ms; inversion times = 50, 150, 300, 600, 1000, 3000 ms; acquisition time of roughly 1.7 min per inversion time (single slice). The acquisition times are given for bilateral axial scans; in one patient the data were acquired in the sagittal plane. B_1 maps were interpolated using data from a single slice (i.e. 2D approach), as described above, from the partial fat B_1 map obtained by calculating the correction factor in Equation (3). The true T_1 of fat was measured using a spectroscopic inversion recovery sequence acquired in voxels containing mostly fat. The IR-PRESS sequences had a TR of 3100 ms, and inversion times of 100, 650, 1050, and 2500 ms, in a 5 mm isotropic voxel, NSA = 4, and an acquisition time of 2.5 min. The accuracy of the T_1 maps obtained from the VFA sequence corrected for variations in B_1 using the reference tissue method was evaluated by comparing the T_1 values in a few regions of interest (ROIs) (drawn in the glandular tissue) to the values for the same ROIs in the maps generated from the IR-FSE data. Scatter plots were formed by plotting the IR T_1 data on one axis and the VFA T_1 on the other, for both uncorrected and B_1 corrected data, on a voxel-by-voxel basis for each patient. A linear function was then fit to the data. The slopes of the resulting fits provided another measure of the performance of the correction. The root-mean-square error

(RMSE) for each fit was calculated to assess the spread of the T_1 data relative to the IR vs. VFA fit.

To determine whether there are significant variations in the T_1 values of breast fat in different patients, single-voxel spectroscopic inversion recovery sequences were acquired in ten patients, using the same acquisition parameters as listed above. The amplitude of the main peak (CH2) of the fat spectrum as a function of inversion time was fit to the inversion recovery signal model to obtain an estimate for the T_1 of adipose tissue in the breast, using in-house software.

In order to estimate the effect of using a population average for the T_1 of fat on the flip angle correction factor 'A', the following equation was solved:

$$\frac{\delta \mathrm{A}_{\mathrm{T1t}}}{\mathrm{A}} = \frac{\delta \mathrm{T}_{1\mathrm{t}}}{\mathrm{A}} \frac{\partial \mathrm{A}}{\partial \mathrm{T}_{1\mathrm{t}}} = -\frac{\delta \mathrm{T}_{1\mathrm{t}} TR e^{-TR/\mathrm{T}_{1\mathrm{t}}}}{\mathrm{T}_{1\mathrm{t}}{}^2 cos^{-1}\left(\mathrm{e}^{-TR/\mathrm{T}_{1\mathrm{t}}}\right) \sqrt{1-\mathrm{e}^{-2TR/\mathrm{T}_{1\mathrm{t}}}}} \quad (6)$$

Where δA_{T1t} is the bias in A from a bias in the assumed true T_1 of fat (δT_{1t}).

Results

Flood phantom

From the spectroscopic inversion recovery data (PRESS-IR), the T_1 of the flood phantom was determined to be 217.3 ms ± 10.3 ms. The T_1 map obtained from the VFA data was used to generate a B_1 map from Equation (3), using the inversion recovery result as the true T_1.

The reference signal B_1 map and the one obtained from the dual TR 'Actual Flip angle Imaging' (AFI) sequence can be seen in Figure 2. Plots of the profile of the map in a medial and posterior line through the phantom 'breasts' can also be seen in the figure. While both B_1 maps generally follow the same trend there are significant differences in their magnitudes in some locations. For the portion of the phantom that corresponds to the breasts only, the absolute difference, averaged across all voxels, between the reference signal B_1 map and the dual TR AFI map was 5.4% ± 5.3%, with an average difference in the top tenth percentile of 17.1% ± 4.4%.

The interpolated maps from the flood phantom tests were compared to the full B_1 map by calculating the mean absolute differences between the full reference signal B_1 map and the interpolated map in the voxels in the regions that were zeroed out (taking the average over all interpolated voxels). Two of the realizations of this experiment are depicted in Figure 3, where the original map, the zeroed out regions, and the resulting interpolated maps (with N = 6, P = 1, 2, 3) can be seen. In these examples the mean absolute difference between the original and interpolated maps are shown for each interpolated map. When the power of the inverse distance-weighting algorithm (Equation 5) was increased, the calculated maps deviated further from the original maps. We determined that linear inverse distance weighting (P = 1) resulted in the most accurate maps in the interpolated regions. For example, in one case the mean differences between the original and interpolated maps

(across all zeroed out voxels) were 5.6%, 6.2% and 6.7%; for P's 1, 2, and 3, respectively. The value of N did not have as large an effect as P on the resulting maps, an N of 6 was selected as it offered a good combination of accuracy and computational efficiency. For example, the mean absolute difference between the original and interpolated maps varied by 0.6% between N values of 1 and 8.

Multiple "tissue" phantom

T_1 values from the inversion recovery, uncorrected and B1-corrected VFA measurements can be seen in Table 1. The results shown in Table 1 are the means (and standard deviations) from all the voxels of that "tissue" type in the slice measured. The compartments were segmented based on signal intensity in the VFA series as well as T_1's resulting from the fits of the uncorrected VFA data. It can be seen that use of the reference tissue B_1 map to correct flip angles reduced the difference between the VFA and IR T_1's in the gelatin and water with contrast media compartments.

In-vivo scans

Reference tissue and interpolated B_1 maps are shown in Figure 4. T_1 maps from one of the cases can be seen in Figure 5. In this figure the overestimation of T_1 values in the parenchyma by the uncorrected VFA data is clearly seen. This figure also shows that the T_1 map produced from the VFA data corrected for local variations in flip angle is closer to the IR map than the uncorrected T_1 map. Results from the four patient scans are summarized in Table 2. The use of interpolated reference tissue B_1 maps for calculations of T_1 from VFA data significantly reduced the difference between the measured 'gold standard' inversion recovery and VFA T_1 values in glandular tissue. Before correction the average absolute difference between VFA and IR values was 58% ± 21% ($p < 0.05$); after correction the absolute difference was reduced to 8.1% ± 7.8% ($p > 0.05$). In the voxels with the top 10% of differences the average was 170% ± 53% without B_1 correction and 28% ± 13% after B_1 correction. In the IR vs. VFA linear fits of the T_1 values in the ROI's analyzed (two examples can be seen in Figure 6), the slope of the B_1 corrected data was closer to 1 for all cases. The root-mean-square error (RMSE) in the VFA vs IR fits was also reduced in all cases following the flip angle correction from the reference tissue B_1 maps, indicating a reduction in the spread of the T_1 values. The average intra-patient standard deviation in the fat T_1 values, as measured from the IR sequence, was 7.9% of the mean.

Spectroscopic fat measurements

The mean fat T_1 value from the spectroscopic measurements in ten patients was 341.3 ms with a standard deviation of 31 ms. Equation 6 was solved to estimate of the bias introduced in 'A' from differences between the true T_1 value in a particular patient, and the population average. A 10% error in the assumed true T_1 of fat led to a relative bias of 5% in the estimate of the flip angle correction factor 'A'. A difference of 10% was chosen due to the fact that the standard deviation in the T_1's measured was 9% of the mean. This relative bias increases with the error in the assumed true T_1.

Discussion and Conclusions

The method proposed here, using a reference signal from a region (or regions) with a known T_1, produced B_1 maps that successfully reduced the variation between T_1 values measured using a variable flip angle and an inversion recovery sequence in the breast parenchyma *in vivo* and in phantom studies.

Significant differences were observed between B_1 maps obtained from solving Equation 3 and the AFI method in some locations in a flood phantom. This is likely due to inadequate spoiling in the implementation of the AFI sequence causing off-resonance artifacts (13).

A linear inverse distance weighted interpolation was shown to accurately recover a full B_1 map when starting with a partial map from a reference region. This was determined in phantom scans using acquisition parameters equivalent to those used in other in-vivo studies.

In a non-uniform phantom built to mimic the T_1 values of breast tissues, a B_1 map was generated by interpolation from the data of one compartment alone (the 'fat' compartment). This map significantly reduced the difference between the T_1's measured with a VFA sequence and the IR results in the gelatin ('parenchyma') compartment. In a third compartment containing an aqueous solution of contrast media, the variability between the VFA and IR results was also reduced, however the remaining difference after correction was larger than in the gelatin compartment. This could be due to local variations in the B_1 field caused by the different dielectric properties of the water and contrast agent compartment, compared to those of the water and gelatin used.

Data from the *in vivo* scans showed a reduction in the difference between IR and VFA T_1's, when the flip angles are corrected using the method presented here. The T_1 values of the parenchyma were overestimated by the non-corrected VFA data in every case. This is likely due to both the deviation from the nominal flip angles, and the difficulty of estimating a relatively long T_1 from VFA data acquired with a short TR. While overall differences between the corrected and IR maps were reduced to 8%; in one of the cases a mean difference greater than 18% remained in the T_1's. In this study we employed a 2D approach for the interpolation of the full map, using data from a single slice to interpolate the B_1 map. Incorporating data from contiguous slices, adding more directions in the interpolation, could potentially increase the accuracy of the method proposed.

Segmentation of the fat in the breast was achieved by using thresholds for signal intensity and the uncorrected T_1. This had the drawback of requiring supervision to avoid errors in segmentation caused by non-uniformity in the signal intensity of fat. An automatic algorithm such as Fuzzy C-means clustering could increase the accuracy of the segmentation (25).

Obtaining a B_1 map using the current approach requires knowledge of the T_1 of a reference tissue, in this case fat. A spectroscopic inversion recovery sequence in a voxel placed in the fat was used to measure the T_1 value in several patient scans. The relatively low standard deviation across all patient scans in this study and previous measurements suggest low inter-patient variability of the T_1 of fat. This suggests that one could forego the measurement of

the T_1 of fat in each patient and use a population average when generating a B_1 map with this approach. This could also be useful in correcting data retrospectively in studies where a T_1 map was acquired but the B_1 field was not mapped. A simple simulation showed that the flip angle correction factor estimated with this method is relatively sensitive, but not overly sensitive, to differences between the actual true T_1 of fat and an assumed value (i.e. population average), with the parameters used here.

Other methods for combined T_1/B_1 mapping have focused on novel acquisition techniques. Treier et al. proposed a method based on a VFA approach incorporating data from a dual TR (AFI) acquisition (26). In this study the authors optimized the acquisition parameters for a dual flip angle VFA for a range of T_1 values (100 – 800 ms) while keeping acquisition times short. Their results showed increased accuracy in T_1 mapping with this approach, and demonstrated its usefulness in DCE-MRI applications. Hurley et al. showed that this method increases the accuracy of T_1 mapping even in the presence of short T_1's, as long as adequate spoiling is performed (27). However, the accuracy of this method may be somewhat limited in areas of the body with a large range of T_1's, such as the breast (28). Due to the reliance of this method on the AFI technique, it also suffers from the shortcomings of the AFI above. Another approach based on the AFI, the multiple TR B_1/T_1 mapping (MTM) method was proposed by Voigt et al. (29). In the MTM the pair of TR's used by the AFI is substituted with a series of TR's; this yields both B_1 and T_1 estimates. The additional TR's increased the accuracy of the AFI method but resulted in increased acquisition times. Another method for the acquisition of combined B_1/T_1 maps, DESPOT1-HIFI, produced combined maps by adding an inversion prepared SPGR image along with the multi flip angle SPGR data acquired in DESPOT1 (30). However this method's accuracy may be limited in areas with long T_1's and affected by error in the inversion pulse it employs. In contrast to these combined B_1/T_1 mapping methods, the reference tissue method proposed here, as well as related methods proposed by Sung et al. (18), relies on post processing of a VFA T_1 map, eliminating the need for specialized acquisitions. However the reference tissue method requires the presence of a tissue with a known, homogeneous T_1 in the field-of-view, ideally surrounding a tissue or area of interest. The abundance and wide distribution of fat makes the breast well suited for this method. The method may also be effective in other regions of the body, e.g. cerebral spinal fluid (CSF) in the brain could be used as a 'reference tissue'. One must exercise caution when selecting a reference tissue so as to avoid partial volume effects, especially in the case of CSF. In some regions use of this approach might be more challenging due to lack of an optimal reference tissue.

In conclusion, we present a method that allows mapping of the B_1 field in a reference region or tissue with a known T_1; the data from this reference tissue can then be used to interpolate the B_1 map in the rest of the tissue of interest. This approach was validated in phantom scans and tested in *in vivo* breast scans. The maps generated with this method reduced the variability in the T_1 values measured with a variable flip angle sequence when compared to inversion recovery values. Accurate knowledge of the flip angle across the field of view is important not only in the quantitation of T_1 values, but also in the quantitative analysis of DCE-MRI data. This method provides a new alternative for mapping the B_1 field in the breast, and requires only the T_1 of the reference tissue, either from direct measurements or

from a population average. While related methods have shown promise, this is the first study that has quantitatively validated a reference tissue post-processing method.

Acknowledgments

Funding Support: Army Breast Cancer Research Program. Grant Number: BC101131. Supported, in part, by the National Institute of Biomedical Imaging and Bioengineering of the National Institutes of Health under grant number T32 EB002103; by the National Cancer Institute of the National Institutes of Health under grant numbers RO1 CA 16778, ROI CA 172801, P30 CA 014599; by the Segal Foundation; by the VPH-PRISM Consortium of the European Union.

References

1. Peters N, Rinkes IB. Meta-Analysis of MR Imaging in the Diagnosis of Breast Lesions. Radiology. 2008:246.
2. Elsamaloty H, Elzawawi MS, Mohammad S, Herial N. Increasing accuracy of detection of breast cancer with 3-T MRI. AJR. Am. J. Roentgenol. 2009; 192:1142–8. [PubMed: 19304726]
3. Kuhl CK, Schrading S, Strobel K, Schild HH, Hilgers R-D, Bieling HB. Abbreviated Breast Magnetic Resonance Imaging (MRI): First Postcontrast Subtracted Images and Maximum-Intensity Projection-A Novel Approach to Breast Cancer Screening With MRI. J. Clin. Oncol. 2014:1–10.
4. Kuhl CK, Mielcareck P, Klaschik S, Leutner C, Wardelmann E, Gieseke J, Schild HH. Dynamic breast MR imaging: are signal intensity time course data useful for differential diagnosis of enhancing lesions?. 1999:101–110.
5. Kuhl CK, Kooijman H, Gieseke J, Schild HH. Effect of B1 inhomogeneity on breast MR imaging at 3.0 T. Radiology. 2007; 244:929–30. [PubMed: 17709843]
6. Azlan, C a; Di Giovanni, P.; Ahearn, TS.; Semple, SIK.; Gilbert, FJ.; Redpath, TW. B1 transmission-field inhomogeneity and enhancement ratio errors in dynamic contrast-enhanced MRI (DCE-MRI) of the breast at 3T. J. Magn. Reson. Imaging. 2010; 31:234–9. [PubMed: 20027594]
7. Willinek WA, Gieseke J, Kukuk GM, Nelles M, König R, Morakkabati-Spitz N, Träber F, Thomas D, Kuhl CK, Schild HH. Dual-source parallel radiofrequency excitation body MR imaging compared with standard MR imaging at 3.0 T: initial clinical experience. Radiology. 2010; 256:966–75. [PubMed: 20720078]
8. Rahbar H, Partridge SC, Demartini WB, Gutierrez RL, Parsian S, Lehman CD. Improved B1 homogeneity of 3 Tesla breast MRI using dual-source parallel radiofrequency excitation. J. Magn. Reson. Imaging. 2012; 35:1222–6. [PubMed: 22282269]
9. Schabel MC, Parker DL. Uncertainty and bias in contrast concentration measurements using spoiled gradient echo pulse sequences. Phys. Med. Biol. 2008; 53:2345–73. [PubMed: 18421121]
10. Tofts PS. Modeling tracer kinetics in dynamic Gd-DTPA MR imaging. J. Magn. Reson. Imaging. 1997; 7:91–101. [PubMed: 9039598]
11. Tofts PS, Brix G, Buckley DL, et al. Estimating Kinetic Parameters from Dynamic Contrast-Enhanced T1 -Weighted MRI of a Diffusable Tracer: Standardized Quantities and Symbols. J. Magn. Reson. Imaging. 1999; 10:223–232. [PubMed: 10508281]
12. Yarnykh VL. Actual flip-angle imaging in the pulsed steady state: a method for rapid three-dimensional mapping of the transmitted radiofrequency field. Magn. Reson. Med. 2007; 57:192–200. [PubMed: 17191242]
13. Nehrke K. On the steady-state properties of actual flip angle imaging (AFI). Magn. Reson. Med. 2009; 61:84–92. [PubMed: 19097210]
14. Cunningham CH, Pauly JM, Nayak KS. Saturated double-angle method for rapid B1+ mapping. Magn. Reson. Med. 2006; 55:1326–1333. [PubMed: 16683260]
15. Nehrke K, Börnert P. DREAM--a novel approach for robust, ultrafast, multislice B_1 mapping. Magn. Reson. Med. 2012; 68:1517–26. [PubMed: 22252850]
16. Sacolick LI, Wiesinger F, Hancu I, Vogel MW. B1 mapping by Bloch-Siegert shift. Magn. Reson. Med. 2010; 63:1315–22. [PubMed: 20432302]

17. Nehrke K, Sprinkart AM, Börnert P. An in vivo comparison of the DREAM sequence with current RF shim technology. Magn. Reson. Mater. Physics, Biol. Med. 2014
18. Sung K, Saranathan M, Daniel BL, Hargreaves BA. Simultaneous T1 and B1 + mapping using reference region variable flip angle imaging. Magn. Reson. Med. 2013; 70:954–961. doi: 10.1002/mrm.24904. PMC3923865. [PubMed: 23943610]
19. Rakow-Penner R, Daniel B, Yu H, Sawyer-Glover A, Glover GH. Relaxation times of breast tissue at 1.5T and 3T measured using IDEAL. J. Magn. Reson. Imaging. 2006; 23:87–91. [PubMed: 16315211]
20. Merchant TE, Thelissen GR, de Graaf PW, Nieuwenhuizen CW, Kievit HC, Den Otter W. Application of a mixed imaging sequence for MR imaging characterization of human breast disease. Acta radiol. 1993; 34:356–361. [PubMed: 8318297]
21. Graham SJ, Ness S, Hamilton BS, Bronskill MJ. Magnetic resonance properties of ex vivo breast tissue at 1.5 T. Magn. Reson. Med. 1997; 38:669–677. [PubMed: 9324335]
22. Fram EK, Herfkens RJ, Johnson GA, Glover GH, Karis JP, Shimakawa A, Perkins TG, Pelc NJ. Rapid calculation of T1 using variable flip angle gradient refocused imaging. Magn. Reson. Imaging. 1987; 5:201–208. [PubMed: 3626789]
23. Deoni SCL. Correction of main and transmit magnetic field (B0 and B 1) inhomogeneity effects in multicomponent-driven equilibrium single-pulse observation of T1 and T2. Magn. Reson. Med. 2011; 65:1021–1035. [PubMed: 21413066]
24. Liney GP, Tozer DJ, Turnbull LW. A simple and realistic tissue-equivalent breast phantom for MRI. J. Magn. Reson. Imaging. 1999; 10:968–71. [PubMed: 10581510]
25. Ahmed MN, Yamany SM, Mohamed N, Farag A a. Moriarty T. A modified fuzzy C-means algorithm for bias field estimation and segmentation of MRI data. IEEE Trans. Med. Imaging. 2002; 21:193–199. [PubMed: 11989844]
26. Treier R, Steingoetter A, Fried M, Schwizer W, Boesiger P. Optimized and combined T1 and B1 mapping technique for fast and accurate T1 quantification in contrast-enhanced abdominal MRI. Magn. Reson. Med. 2007; 57:568–76. [PubMed: 17326175]
27. Hurley, S a; Yarnykh, VL.; Johnson, KM.; Field, AS.; Alexander, AL.; Samsonov, A a. Simultaneous variable flip angle-actual flip angle imaging method for improved accuracy and precision of three-dimensional T1 and B1 measurements. Magn. Reson. Med. 2012; 68:54–64. [PubMed: 22139819]
28. Bottomley, P a. A review of 1H nuclear magnetic resonance relaxation in pathology: Are T1 and T2 diagnostic? Med. Phys. 1987; 14:1. [PubMed: 3031439]
29. Voigt T, Nehrke K, Doessel O, Katscher U. T1 corrected B1 mapping using multi-TR gradient echo sequences. Magn. Reson. Med. 2010; 64:725–733. [PubMed: 20564577]
30. Deoni SCL. High-resolution T1 mapping of the brain at 3T with driven equilibrium single pulse observation of T1 with high-speed incorporation of RF field inhomogeneities (DESPOT1-HIFI). J. Magn. Reson. Imaging. 2007; 26:1106–1111. [PubMed: 17896356]

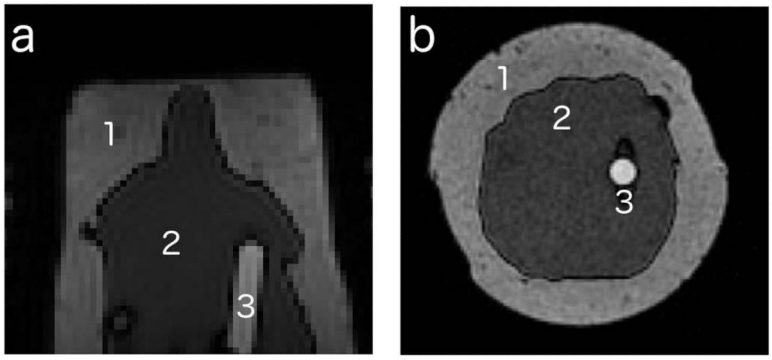

Figure 1.
Cross-sections of the non-uniform phantom in the (a) axial and (b) coronal planes, 3 regions can be seen in each one: (1) lard, (2) gelatin, and (3) water + contrast media

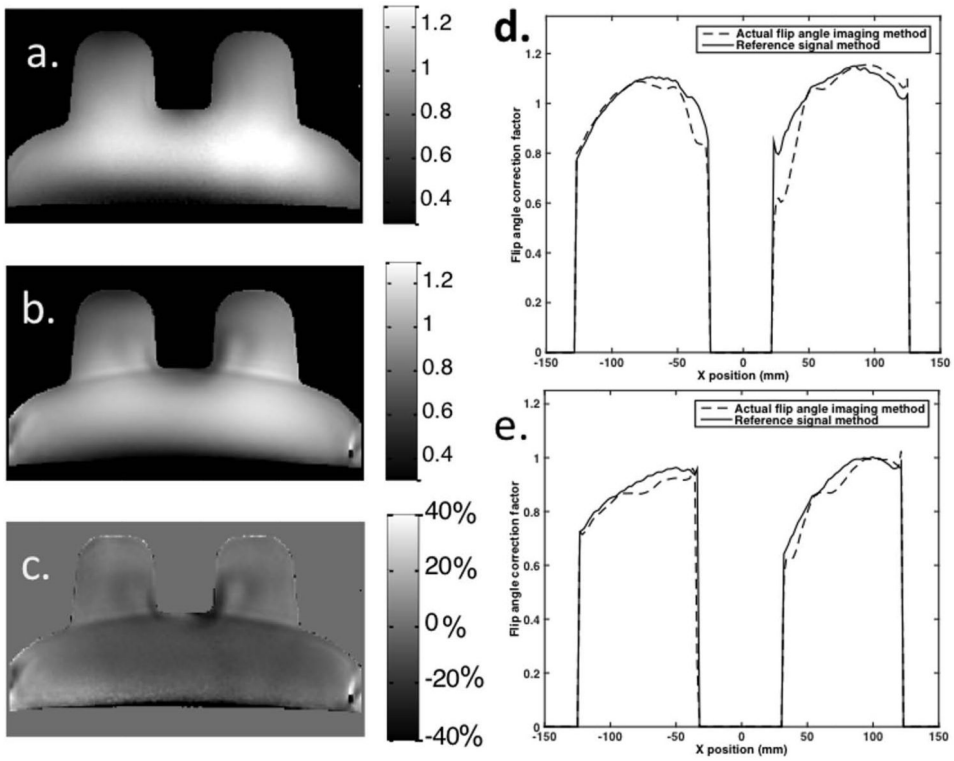

Figure 2.

B_1 maps for a flood phantom from (a) reference signal method and (b) dual TR actual flip angle imaging sequence, along with a percent difference image (c) between the two (scale for a and b corresponds to the correction factor between the nominal and actual flip angle). On the right, profile plots of the B_1 maps obtained in a flood phantom for lines through the (d) central and (e) posterior section of the 'breasts'

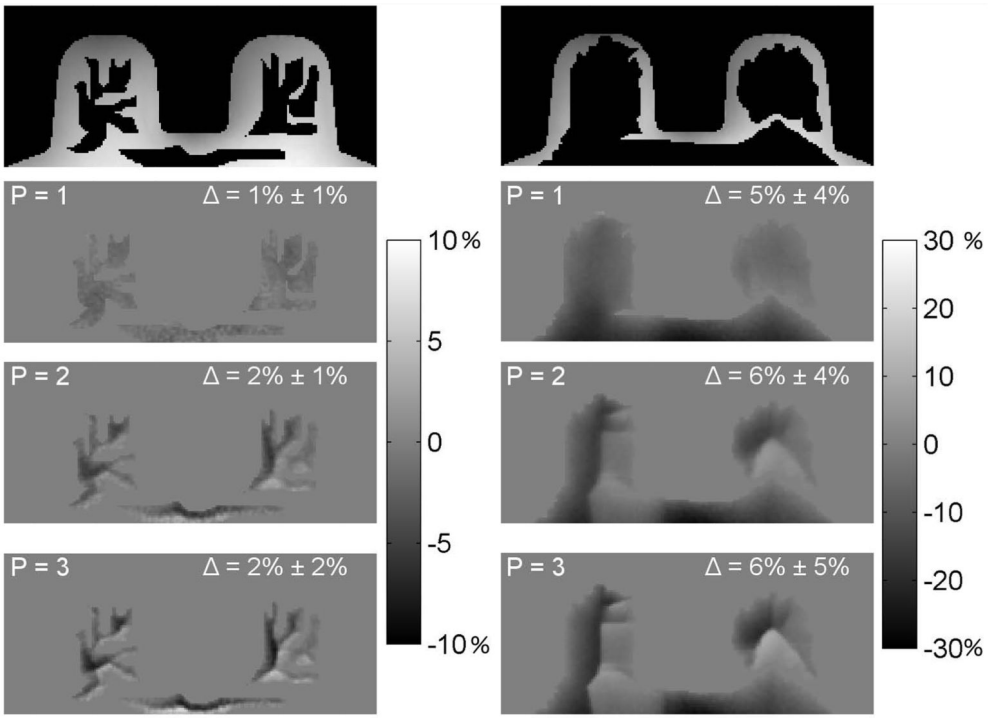

Figure 3.

Examples of the interpolation tests in a flood phantom for two different simulated fat distributions. Top row: maps with zeroed-out regions. The bottom 3 rows depict percent difference images between the original and interpolated maps, for different values of the power of the inverse distance weighting (P). The value of Δ is the mean absolute difference (in the zeroed-out regions) between the original and interpolated maps (± standard deviations)

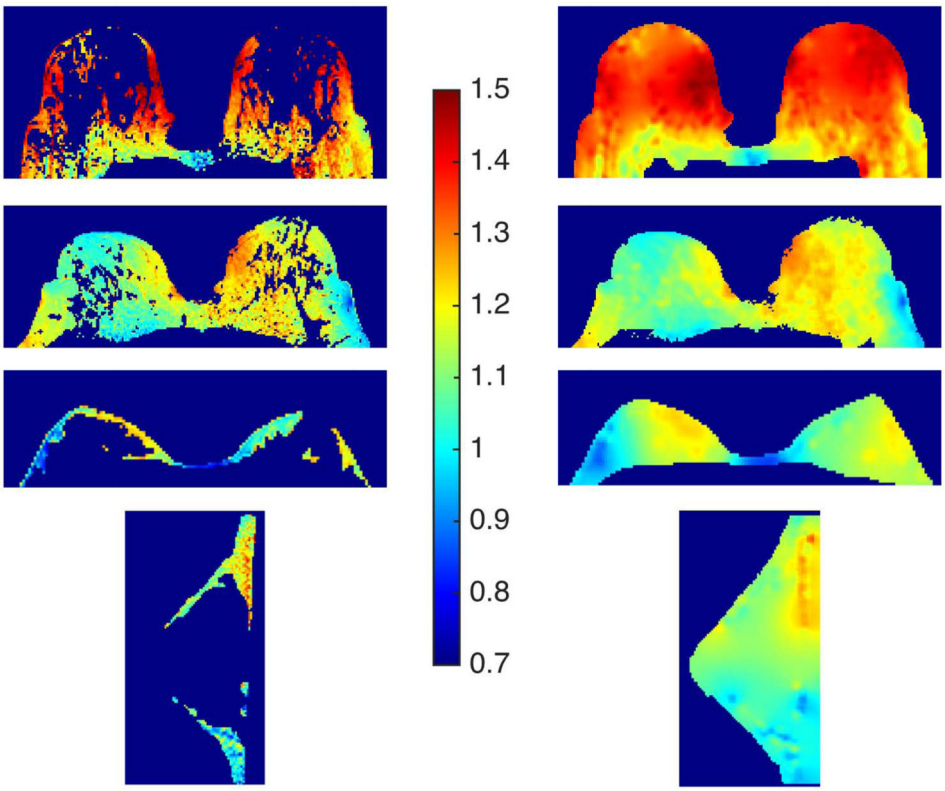

Figure 4.

In vivo results, B_1 maps for the reference tissue (left column) and interpolated maps for the whole breast (right column); displayed in terms of the flip angle correction factor ('A'). The bottom row were acquired from a unilateral sagittal scan, all others were acquired axially.

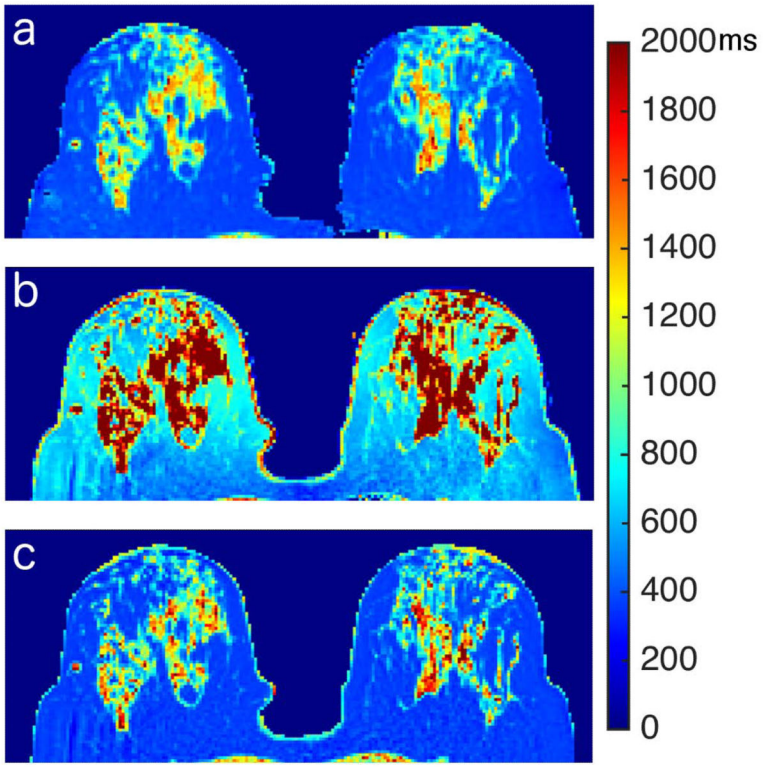

Figure 5.

T_1 maps from an *in vivo* scan: a) inversion recovery T_1 map; b) uncorrected VFA T_1 map; c) VFA T_1 map corrected with interpolated B_1 map

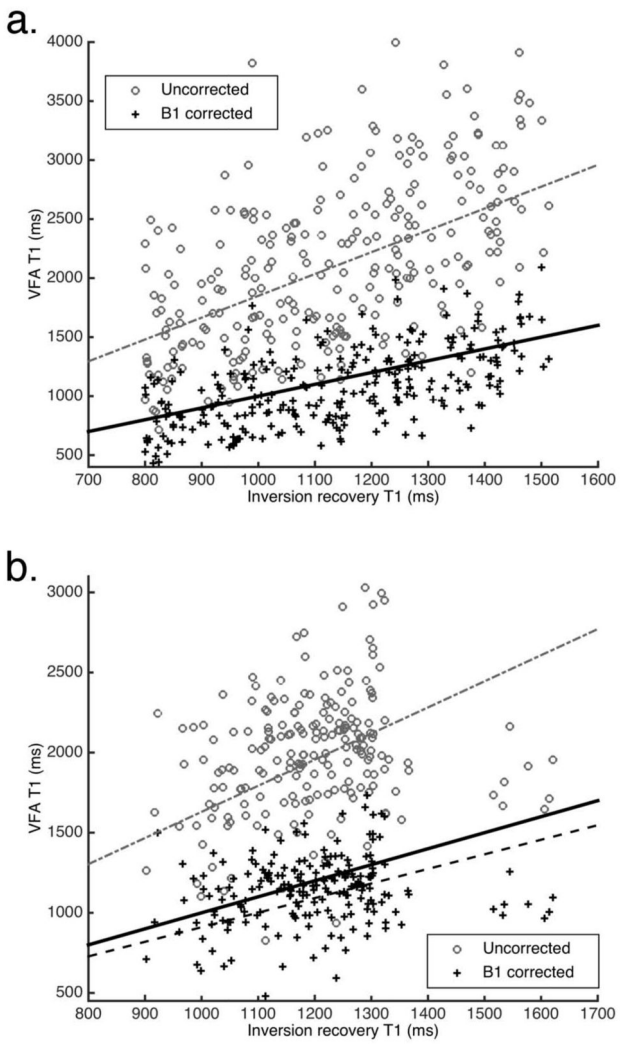

Figure 6.

Scatter-plots of VFA T_1 data (before and after B1 correction) vs. inversion recovery T_1 data. Dotted lines correspond to linear fits to data, solid line is the line of equality (lines overlap in a). Parameters for the fits are included in Table 2 (a. case 1, b. case 2)

Table 1

T_1 measurements (before and after B_1 correction) from the multiple compartment phantom

Compartment	IR T_1 (ms)	Uncorrected VFA T_1 (ms)	Difference	B_1 corrected VFA T_1 (ms)	Difference
Lard	246.9 ± 11.9	267.4 ± 45.4	8.3%	256.3 ± 13.8	3.8%
Gelatin	2009.2 ± 44.9	2543.6 ± 295.9	26.6%	2070.5 ± 235.3	3.1%
Water + CA	708.1 ± 27.9	903.61 ± 31.5	27.6%	803.5 ± 28	13.5%

Table 2

In vivo T_1 measurements performed at 3T for: inversion recovery, VFA (before and after B_1 correction) and fit parameters for IR vs VFA scatter-plots.

#	IR T_1 (ms)	VFA T_1 (ms)		% Difference in T_1		IR T_1 vs VFA T_1 fits			
						Slope		RMSE (ms)	
		No correction	B_1 corrected	No correction	B_1 corrected	No correction	B_1 corrected	No correction	B_1 corrected
1	1145 ± 228	2119 ± 751	1147 ± 401	85.1%	0.2%	1.85	1.00	622	335
2	1145 ± 123	1878 ± 345	1049 ± 226	64.0%	−8.4%	1.63	0.91	348	236
3	942 ± 239	1269 ± 508	894 ± 420	34.7%	−5.1%	1.32	1.15	483	403
4	1074 ± 219	1610 ± 451	1274 ± 323	49.9%	18.6%	1.49	1.18	335	225